

Magnetocrystalline anisotropy of Fe_5PB_2 and its alloys with Co and $5d$ elements: a combined first-principles and experimental study

Mirosław Werwiński*

*Institute of Molecular Physics, Polish Academy of Sciences,
M. Smoluchowskiego 17, 60-179 Poznań, Poland*

Alexander Edström

Materials Theory, ETH Zürich, Wolfgang-Pauli-Str. 27, 8093 Zürich, Switzerland

Ján Ruzs

Department of Physics and Astronomy, Uppsala University, Box 516, SE-751 20 Uppsala, Sweden

Daniel Hedlund, Klas Gunnarsson, and Peter Svedlindh

Department of Engineering Sciences, Uppsala University, Box 534, SE-751 21 Uppsala, Sweden

Johan Cedervall and Martin Sahlberg

*Department of Chemistry – The Ångström Laboratory,
Uppsala University, Box 538, SE-751 21 Uppsala, Sweden*

(Dated: March 14, 2022)

The Fe_5PB_2 compound offers tunable magnetic properties via the possibility of various combinations of substitutions on the Fe and P-sites. Here, we present a combined computational and experimental study of the magnetic properties of $(\text{Fe}_{1-x}\text{Co}_x)_5\text{PB}_2$. Computationally, we are able to explore the full concentration range, while the real samples were only obtained for $0 \leq x \leq 0.7$. The calculated magnetic moments, Curie temperatures, and magnetocrystalline anisotropy energies (MAEs) are found to decrease with increasing Co concentration. Co substitution allows for tuning the Curie temperature in a wide range of values, from about six hundred to zero kelvins. As the MAE depends on the electronic structure in the vicinity of Fermi energy, the geometry of the Fermi surface of Fe_5PB_2 and the \mathbf{k} -resolved contributions to the MAE are discussed. Low temperature measurements of an effective anisotropy constant for a series of $(\text{Fe}_{1-x}\text{Co}_x)_5\text{PB}_2$ samples determined the highest value of 0.94 MJ m^{-3} for the terminal Fe_5PB_2 composition, which then decreases with increasing Co concentration, thus confirming the computational result that Co alloying of Fe_5PB_2 is not a good strategy to increase the MAE of the system. However, the relativistic version of the fixed spin moment method reveals that a reduction in the magnetic moment of Fe_5PB_2 , by about 25%, produces a fourfold increase of the MAE. Furthermore, calculations for $(\text{Fe}_{0.95}\text{X}_{0.05})_5\text{PB}_2$ ($\text{X} = 5d$ element) indicate that 5% doping of Fe_5PB_2 with W or Re should double the MAE. These are results of high interest for, e.g., permanent magnet applications, where a large MAE is crucial.

PACS numbers: 71.20.Be, 75.30.Gw, 75.50.Bb, 75.50.Cc, 75.50.Ww

I. INTRODUCTION

Many sectors of modern technology depend on magnetic materials, which are used in such ubiquitous applications as electric motors, power generators, transformers, and recording media. Hence, magnetic materials are crucial, not only for the digital technology revolution observed in past decades, but also for the green energy revolution expected within the years to come. The fundamentally and technologically most important intrinsic parameters of magnetic materials include the Curie temperature (T_C), saturation magnetization (M_S), and magnetocrystalline anisotropy energy (MAE). These parameters are important in a wide variety of applications, including hard and soft magnetic materials for energy conversion, spintronics, and information storage. Thus, the ability to predict these basic magnetic parameters from first principles is of utmost importance, and accu-

rate modern electronic structure calculations provide an indispensable tool for exploring new materials with desired properties. In parallel, experimental synthesis and characterization retains its fundamental importance and a close interplay between computational and experimental work is of ever increasing value in modern materials discovery.

One example of an area in which the search for new magnetic materials, with specific combinations of properties, has been intense in recent years is that of permanent magnets. In this field it is typically desirable to have large M_S , T_C and MAE. This combination is obtained in the commonly used rare-earth transition metal compounds, such as $\text{NdFe}_{14}\text{B}_2$. However, the so called *Rare-Earth Crisis*¹ triggered immense international research initiatives in search for new substitute permanent magnet materials with reduced amounts of, or no, rare-earth elements²⁻⁶. The main challenge in this context is obtaining a sufficiently large MAE in transition metal

compounds, where a uniaxial (e.g. tetragonal or hexagonal) crystal structure is a crucial prerequisite. Other areas of applications depend upon other combinations of properties. For example, for magnetocaloric solid state cooling, it is desirable to be able to tune the ordering temperature such that it coincides with the operating temperature (often room temperature)^{7,8}.

Various works have shown how strain engineering or alloying can be used to carefully tune the properties of magnetic materials to obtain desired functionality. For example, it was shown that a careful control of strain and alloy concentration allows for a large MAE in bct FeCo alloys^{9–12}. The potential route to FeCo-based permanent magnets offered by that work inspired subsequent studies aiming to stabilize tetragonality in FeCo by B or C-impurities^{13–15}. Also the tetragonal $(\text{Fe}_{1-x}\text{Co}_x)_2\text{B}$ compound has been carefully studied due to its tunable MAE as function of x ^{16–20} which, furthermore, has an intriguing temperature dependence^{19,21,22}. It was also shown, in both calculations and experiments, that small amounts of $5d$ substitutions on the Fe/Co site allowed a large increase in the MAE of this material¹⁹.

The tetragonal family of compounds with compositions $(\text{Fe}_{1-x}\text{Co}_x)_5\text{P}_{1-y}\text{Si}_y\text{B}_2$ has also been the subject of numerous recent studies^{23–28}. Additionally, other chemical substitutions, including Mn on the Fe/Co site²³, have been considered. Due to the broad range of chemical compositions available, this material offers wide tunability of its magnetic properties. Furthermore, the tetragonal crystal structure could potentially allow for a large MAE and, thus, make the compounds interesting within the context of permanent magnet applications. The materials also exhibit other interesting aspects, such as the temperature dependent spin-reorientation transition in Fe_5SiB_2 ²⁵.

The aim of the work is to investigate the effect of the Co and $5d$ dopants on the tunable magnetic properties of the technologically promising semi-hard Fe_5PB_2 compound. Fe_5PB_2 crystallizes in the Cr_5B_3 -type structure with a body-centered tetragonal (bct) unit cell, space group $I4/mcm$ ²⁹ (see Fig. 1). The unit cell of Fe_5PB_2 consists of 4 formula units (32 atoms). Fe atoms occupy two inequivalent sites Fe_1 (16l) and Fe_2 (4c). Fe_1 atoms are distributed on the 16-fold position, Fe_2 and P on the 4-fold, and B on the 8-fold position.

One of the motivations to investigate the $(\text{Fe}_{1-x}\text{Co}_x)_5\text{PB}_2$ system are our previous results for isostructural $(\text{Fe}_{1-x}\text{Co}_x)_5\text{SiB}_2$ system (with Si in place of P), for which we have predicted the highest MAE = 1.16 MJ m^{-3} for Co concentration $x = 0.3$.²⁴ Next, the $(\text{Fe}_{0.8}\text{Co}_{0.2})_5\text{SiB}_2$ sample (with Co concentration $x = 0.2$) was synthesized by McGuire and Parker²³ and their magnetic measurements showed an increase of the anisotropy field after Co substitution, which supports our prediction. All the previous experimental studies conducted on the $(\text{Fe}_{1-x}\text{Co}_x)_5\text{SiB}_2$ system are limited to the Fe-rich compositions, while Co_5SiB_2 is not known to form.²³ For melt-spun samples $\text{Fe}_5(\text{Si}_{0.75}\text{Ge}_{0.25})\text{B}_2$

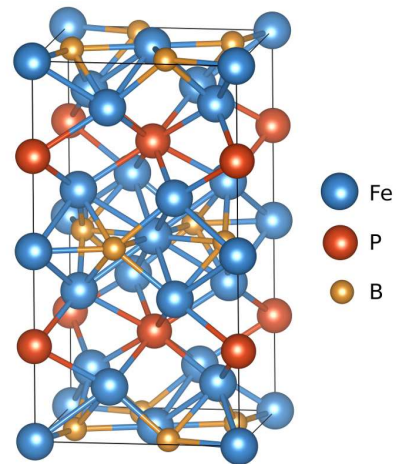


FIG. 1. The crystal structure of Fe_5PB_2 , space group $I4/mcm$ (no. 140).

Lejeune et al. were determined a relatively high anisotropy constant K_1 of about 0.5 MJ m^{-3} at room temperature, which is about double the value for Fe_5SiB_2 .^{24,30} Recently, we also presented a combined experimental and theoretical study of the $\text{Fe}_5\text{Si}_{1-x}\text{P}_x\text{B}_2$ system, which showed the highest anisotropy constant for the terminal Fe_5PB_2 composition.²⁷

Fe_5PB_2 has high T_C of about $655 \pm 2 \text{ K}$, magnetic moment of $1.72 \mu_B/\text{Fe atom}$ ($8.60 \mu_B/\text{f.u.}$), and anisotropy constant K_1 of 0.50 MJ m^{-3} measured at 2 K for single crystal.²⁶ The value of an effective anisotropy constant K_{eff} of Fe_5PB_2 obtained in our previous work is however significantly higher and equal to $\sim 0.9 \text{ MJ m}^{-3}$ at 10 K.²⁷ An important parameter, in context of permanent magnets, is magnetic hardness, defined as:

$$\kappa = \sqrt{\frac{|K|}{\mu_0 M_S^2}}, \quad (1)$$

where K is the magnetic anisotropy constant and M_S is the saturation magnetization. An empirical rule $\kappa > 1$ specifies whether the material have a chance to resist self-demagnetization.⁴ From the experimental values of $K_{\text{eff}} \sim 0.65 \text{ MJ m}^{-3}$ and $M_S = 0.87 \text{ MA/m}$ ²⁷, we determined for Fe_5PB_2 $\kappa = 0.69$ (at 300 K). It implies, that without a further engineering of the anisotropy constant, Fe_5PB_2 will stay in a category of semi-hard magnets.⁴

In this work we consider alloying of Fe_5PB_2 with Co and $5d$ elements. In our recent study of $(\text{Fe}_{1-x}\text{Co}_x)_5\text{PB}_2$ alloys we observed a reduction in magnetization and Curie temperature with an increase of Co concentration.²⁸ McGuire and Parker also found that 20% Co alloying in $(\text{Fe}_{1-x}\text{Co}_x)_5\text{PB}_2$ leads to decrease in magnetization, Curie temperature and anisotropy field.²³ Previously we showed also that increase of the MAE of $3d$ alloys can be achieved through doping with $5d$ elements.¹⁹ In this work we follow this idea and calculate the resultant MAEs of Fe_5PB_2 -based alloys with 5% substitutions

of each $5d$ element in place of Fe.

II. COMPUTATIONAL AND EXPERIMENTAL DETAILS

A. Computational Details

The electronic band structure calculations for $(\text{Fe}_{1-x}\text{Co}_x)_5\text{PB}_2$ and $(\text{Fe}_{0.95}\text{X}_{0.05})_5\text{PB}_2$ ($X = 5d$ element) systems were carried out with use of the full-potential local-orbital electronic structure code FPLO14.0-49³¹ using a fixed atomic-like basis set. The FPLO was an optimal choice for the accurate calculations of MAE due to the full potential and fully relativistic character of the code. To model the Co and $5d$ alloying we used the supercell method. The generalized gradient approximation (GGA) was used in the Perdew-Burke-Ernzerhof form (PBE).³² A $16 \times 16 \times 16$ \mathbf{k} -mesh was found to lead to well converged results of the MAE. For \mathbf{k} -point integration, the tetrahedron method was used.³³ The energy and charge density convergence criteria of $\sim 10^{-7}$ eV and 10^{-6} , respectively, were applied simultaneously. The lattice parameters and Wyckoff positions were optimized for Fe_5PB_2 and Co_5PB_2 within a spin-polarized scalar-relativistic approach. The crystallographic parameters for compositions with intermediate Co concentrations were taken from calculations of full lattice relaxation carried out previously in virtual crystal approximation.²⁸ For the $(\text{Fe}_{0.95}\text{X}_{0.05})_5\text{PB}_2$ supercells we used the same crystallographic parameters as for the Fe_5PB_2 . The MAE was evaluated as a difference between the fully relativistic total energies calculated for quantization axes [100] and [001]. In the adopted sign convention the positive sign of MAE corresponds to an easy magnetization axis along the [001] direction. The Fermi surface (FS) of Fe_5PB_2 was calculated on a 28^3 \mathbf{k} -mesh in a boundary of the first Brillouin zone. Using the fully relativistic fixed spin moment (FSM) scheme³⁴ we study the MAE as a function of total magnetic moment (m) for Fe_5PB_2 . A supercell method was used to model the chemical disorder.^{18,35} To build a supercell, multiplication of the basal unit cell and replacement of an appropriate amount of atoms of one type by atoms of the other type were made. The Fe atoms were replaced by Co or $5d$ atoms forming the $(\text{Fe}_{1-x}\text{Co}_x)_5\text{PB}_2$ and $(\text{Fe}_{0.95}\text{X}_{0.05})_5\text{PB}_2$ compositions ($X = 5d$ element). For $(\text{Fe}_{1-x}\text{Co}_x)_5\text{PB}_2$ the considered intermediate compositions were: $x = 0.2, 0.4, 0.6,$ and 0.8 . The MAE calculations based on the supercell method¹⁸ are uncommon, as they are time-consuming even for relatively simple alloys. The reason for that is significant increase in the number of inequivalent atomic positions generated for the supercell model. Additionally, accurate results require averaging over several different large supercells.^{18,36} It limits the size of supercells which we can use for MAE calculations. Hence, we study only the supercells including symmetry operations and consisting of up to 16 inequiv-

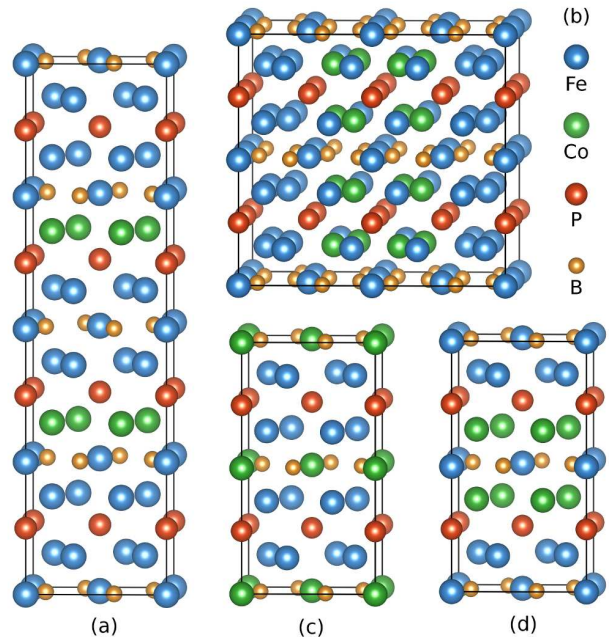


FIG. 2. The crystal structures of the $(\text{Fe}_{1-x}\text{Co}_x)_5\text{PB}_2$ supercells. (a-c) Three configurations of $\text{Fe}_4\text{Co}_1\text{PB}_2$ and (d) single configuration for $\text{Fe}_3\text{Co}_2\text{PB}_2$.

alent atoms. The considered crystal structures are presented in Fig. 2. Three configurations were considered for $\text{Fe}_4\text{Co}_1\text{PB}_2$ and $\text{Fe}_1\text{Co}_4\text{PB}_2$ and one for $\text{Fe}_3\text{Co}_2\text{PB}_2$ and $\text{Fe}_2\text{Co}_3\text{PB}_2$ compositions. For the considered supercell models, the energy convergence with a number of \mathbf{k} -points was carefully tested. The supercell method was also employed to calculate the MAE of $(\text{Fe}_{0.95}\text{X}_{0.05})_5\text{PB}_2$ compositions with various $5d$ elements X . To construct the models, one of twenty Fe atoms in the basal Fe_5PB_2 supercell was replaced by the dopant. It led to the crystal structures containing 10 inequivalent atomic positions. For calculations of the systems with $5d$ dopants a relatively dense $20 \times 20 \times 10$ \mathbf{k} -mesh was used, in order to get the well converged results of MAE.

To compute the Curie temperatures within the mean-field theory (T_C^{MFT}) for the whole series of $(\text{Fe}_{1-x}\text{Co}_x)_5\text{PB}_2$ compositions the FPLO5.00 version of the code was used.³⁷ The T_C^{MFT} is proportional to the total energy difference between the ferromagnetic and paramagnetic configurations³⁸⁻⁴⁰ according to:

$$k_B T_C^{\text{MFT}} = \frac{2}{3} \frac{E_{\text{DLM}} - E_{\text{FM}}}{c}, \quad (2)$$

where E_{DLM} and E_{FM} are total energies for the paramagnetic and ferromagnetic configurations, k_B is Boltzmann constant, and c is total concentration of magnetic atoms. In case of Fe_5PB_2 containing five Fe atoms (considered as magnetic ones) within a formula unit consisting of eight atoms, the concentration parameter c is equal $5/8$. To model the paramagnetic state the disordered local moment (DLM) method was used,⁴¹ in which the thermal disorder among the magnetic moments is modeled

by using the coherent potential approximation (CPA).⁴² The FPLO5 is the latest public version of the code allowing for the CPA calculations and does not have implemented the GGA. Thus, the local density approximation (PW92)⁴³ form of the exchange-correlation potential had to be chosen. For the calculations within FPLO5, a scalar-relativistic mode and a $12 \times 12 \times 12$ \mathbf{k} -mesh were used. In the FPLO5 the magnetically ordered state (resulting in E_{FM}) was artificially modeled within the CPA, to avoid numerical discrepancies between the ordered (in principle non-CPA) and DLM (CPA) models. In calculations using the FPLO5 code, the minimum basis have been optimized for the terminal compositions Fe_5PB_2 and Co_5PB_2 , subsequently the resultant compression parameters were used for intermediate compositions modeled with CPA. The VESTA code was used for visualization of crystal structure.⁴⁴

B. Experimental Details

The samples in the series $(\text{Fe}_{1-x}\text{Co}_x)_5\text{PB}_2$ (x from 0.0 to 0.7) were synthesized by mixing stoichiometric amounts of the master alloys Fe_5PB_2 and Co_5PB_2 . The master alloys were prepared, in accordance with previous studies²⁷, from pure elements of iron (Leico Industries, purity 99.995%, surface oxides reduced in H_2 -gas), cobalt (Johnson Matthey, purity 99.999%), phosphorus (Cerac, purity 99.999%), and boron (Wacher-Chemie, purity 99.995%). This was done by forming first the TM_2B ($\text{TM} = \text{Fe}, \text{Co}$), using a conventional arc furnace, and subsequently dropping the phosphorus in a melt of the metal boride in an induction furnace using the drop synthesis method.⁴⁵ All samples were subsequently crushed, pressed into pellets, and heat treated in evacuated silica ampules at 1273 K for 14 days after which they were quenched in cold water. At x higher than 0.7 the correct crystalline phase could not be produced, all attempts resulted in a decomposition to other crystalline phases.

To study the phase content and to perform crystal structure analysis of all samples, a powder X-ray diffraction (XRD) was used. The measurements were done using a Bruker D8 diffractometer equipped with a LynxEye position sensitive detector (4° opening) using $\text{CuK}\alpha_1$ radiation ($\lambda = 1.540598 \text{ \AA}$) at 298 K in a 2θ range of 20° – 90° . The crystal structures were evaluated with the software FullProf⁴⁶ using refinements according to the Rietveld method.⁴⁷ The unit cell parameters were precisely studied using the least square refinements of the peak positions, employing the software UnitCell.⁴⁸

The synthesized samples were magnetically studied using a Quantum Design PPMS 6000. Samples were immobilized in gelatin capsules with varnish. The magnetization at 3 K was measured between applied magnetic fields of 0 and 7.2 MA m^{-1} . The magnetization in SI units was calculated from magnetic moment using the sample weight and the crystallographic volume obtained

from the XRD measurements at 298 K. When approaching magnetic saturation the magnetization process is described by the law of approach to saturation (LAS).⁴⁹ LAS has been formulated in several ways^{49–52}, but it takes a general form

$$\frac{M}{M_S} = \sum_j a_j H^j, \quad (3)$$

where j is usually an integer, a_j are coefficients, M and M_S are magnetization and saturation magnetization, and H is the applied magnetic field. The LAS was used to determine an effective anisotropy constant $|K_{\text{eff}}|$ in the same implementation as we used before.^{25,27} The interval 93%–98% of the magnetic saturation was used. The applied formula was

$$\frac{M}{M_S} = 1 + aH + \frac{b}{H} + \frac{c}{H^2}. \quad (4)$$

The experimental data was fit with four models in which a and b coefficients can be zero or non-zero and since $\frac{1}{H^2}$ term is used to extract $|K_{\text{eff}}|$ this part is always considered as non-zero. $|K_{\text{eff}}|$ is given here by

$$|K_{\text{eff}}| = \sqrt{\frac{15c}{4}} \mu_0 M_S. \quad (5)$$

The difference in results between all four models are relatively small (max. 0.20 MJ m^{-3}), thus in the experimental section we present only the $|K_{\text{eff}}|$ for the simplest model with the coefficients $a = b = 0$.

III. RESULTS AND DISCUSSION

The results of first-principles calculations of technologically important magnetic parameters for the considered systems are shown. For $(\text{Fe}_{1-x}\text{Co}_x)_5\text{PB}_2$ the M_S , T_C , and MAE are presented. For $(\text{Fe}_{0.95}\text{X}_{0.05})_5\text{PB}_2$ ($X = 5d$ element) the results are limited to MAE and partial magnetic moments. For the main phase – Fe_5PB_2 – a detailed analysis of electronic structure, magnetic moments, Fermi surface, and MAE is given. The theoretical efforts are complemented by experimental synthesis and measurements of the considered $(\text{Fe}_{1-x}\text{Co}_x)_5\text{PB}_2$ compositions.

A. Crystal Structure and Electronic Structure of Fe_5PB_2 and Co_5PB_2

The optimized crystallographic parameters of Fe_5PB_2 and Co_5PB_2 are compared in Table I with the results of measurements. For Fe_5PB_2 the agreement between the GGA and experiment is good and for the Co_5PB_2 the GGA underestimates a and overestimates c . The disagreement may originate from both theory and experiment. The lattice parameters of Co_5PB_2 were last refined by Rundqvist back in 1962.²⁹ Unfortunately, we did

TABLE I. The optimized crystallographic parameters for Fe_5PB_2 and Co_5PB_2 as calculated with the FPLO14 code, using the GGA(PBE) functional, with (SP) and without (NM) spin polarization. Space group $I4/mcm$, no. 140. The Wyck-off positions are: Fe_1/Co_1 ($x, x+1/2, z$), Fe_2/Co_2 ($0, 0, 0$), P ($0, 0, 1/4$), and B ($x, x+1/2, 0$). For comparison the values measured in this work at room temperature for Fe_5PB_2 and the literature values for Co_5PB_2 are also reported.

system	a [Å]	c [Å]	$x_{\text{Fe}_1/\text{Co}_1}$	$z_{\text{Fe}_1/\text{Co}_1}$	x_{B}	c/a
Fe_5PB_2 (GGA-SP)	5.456	10.296	0.170	0.139	0.381	1.887
Fe_5PB_2 (expt.)	5.492	10.365	0.170	0.141	0.381	1.887
Co_5PB_2 (GGA-SP)	5.284	10.541	0.169	0.142	0.376	1.995
Co_5PB_2 (GGA-NM)	5.309	10.406	0.169	0.141	0.376	1.960
Co_5PB_2 (expt.) ²⁹	5.42	10.20	-	-	-	1.882

not manage to synthesize the Co_5PB_2 sample. According to comprehensive study of Haas *et al.* the PBE remains the best GGA functional for most of the solids containing 3d transition elements.⁵³ However, it has a tendency to overestimate the lattice constants.⁵³ The presented PBE results for Fe_5PB_2 go against this trend. PBE underestimates also a volume of Co_5PB_2 . The observed underestimation of lattice parameters/volumes is similar to the results obtained from GGA for bcc Fe⁵⁴ and fcc Co⁵⁵, for which the use of GGA leads to about 0.5 - 1.0% underestimation of the lattice parameters (which is equivalent to about 1.5 - 3.0% underestimation in volume). In case of Fe_5PB_2 and Co_5PB_2 the calculated (with spin polarization) PBE volumes are 2.2 and 1.8% underestimated, respectively. It is surprising, however, that when the c/a ratio for Fe_5PB_2 is in agreement with experiment (both values are equal to 1.887), the corresponding result for Co_5PB_2 from (spin polarized) GGA is significantly different (1.995 against the experimental value 1.882). The non-magnetic GGA calculations leads for Co_5PB_2 to c/a equal to 1.960 – also significantly different from the measured value. We can only give a very general explanation for this discrepancy as coming from the insufficient treatment of corrections in PBE functional.

The spin projected partial and total densities of states (DOS) for Fe_5PB_2 and Co_5PB_2 are presented in Fig. 3. The valence bands of these two metallic systems start around -9 eV. In a range from -9 to -3 eV the main contributions to a valence band come from the P 3p and B 2p orbitals, while from -5 eV up to above E_{F} the dominant role play the 3d orbitals. The observed spin splitting (proportional to the magnetic moment) is bigger for Fe_5PB_2 than for Co_5PB_2 , which is related to a higher filling of the valence band for Co_5PB_2 than for Fe_5PB_2 . The majority spin channels of the two compounds are similar and nearly completely occupied. The additional electrons in the Co_5PB_2 fill mainly the minority spin channel, reducing the magnetic moment. The weak spin polarization of the P 3p and B 2p orbitals is induced by the 3d orbitals. The spin polarization on the Fermi level is defined as $P = \left| \frac{D_{\text{u}} - D_{\text{d}}}{D_{\text{u}} + D_{\text{d}}} \right|$, where D_{u} is the density of states at the Fermi level of the majority spin

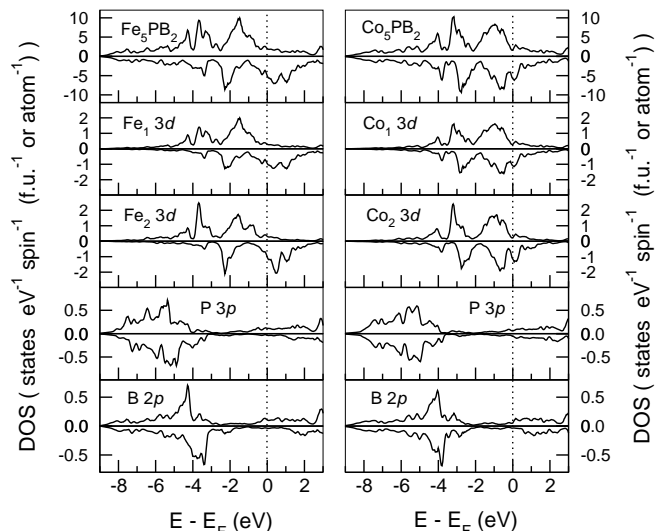


FIG. 3. The spin projected partial and total densities of states (DOS) for Fe_5PB_2 and Co_5PB_2 . Calculations were done within the FPLO14 code using the PBE functional and treating the relativistic effects in a full 4-component formalism (including spin-orbit coupling).

channel, and D_{d} for the minority spin channel. The calculated spin polarization on the Fermi level (a total value including Fe, Co, P, and B contributions) is about 0.46 for Fe_5PB_2 and 0.60 for Co_5PB_2 .

B. Magnetic Moments of $(\text{Fe}_{1-x}\text{Co}_x)_5\text{PB}_2$

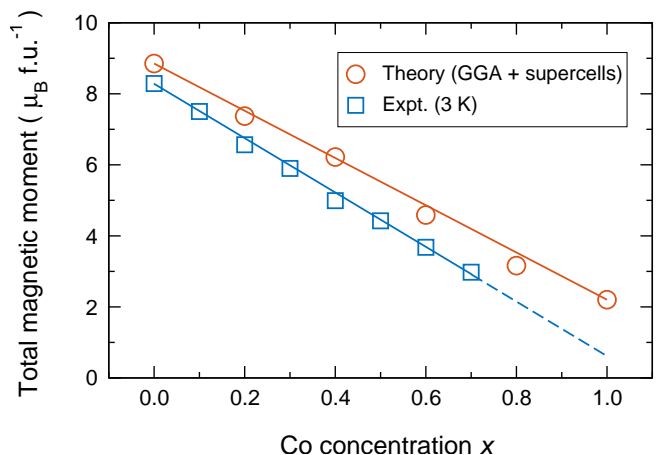


FIG. 4. The Co concentration dependence of total magnetic moment for the $(\text{Fe}_{1-x}\text{Co}_x)_5\text{PB}_2$ system. The results calculated with supercell method are denoted by red circles, the results measured at 3 K by blue squares.²⁸ Linear fits are drawn for a better perception. Calculations were done with the FPLO14 code, using the GGA functional (PBE), and treating the relativistic effects in a full 4-component formalism (including spin-orbit coupling).

TABLE II. The spin, orbital, and total magnetic moments (μ_B (atom or f.u.) $^{-1}$) for Fe_5PB_2 and Co_5PB_2 as calculated along the quantization axis [001] (easy axis) with the FPLO14 code using the PBE functional and treating the relativistic effects in a full 4-component formalism (including spin-orbit coupling). The saturation magnetization M_S (MA m^{-1}) is evaluated based on the total magnetic moments m and theoretical lattice parameters.

site	Fe_5PB_2		Co_5PB_2	
	m_s	m_l	m_s	m_l
$3d_1$	1.78	0.033	0.41	0.011
$3d_2$	2.11	0.052	0.64	0.013
P	-0.13	0.002	-0.02	0.001
B	-0.21	0.001	-0.05	0.000
m	8.85		2.20	
M_S	1.07		0.28	

The calculated Co concentration dependence of the total magnetic moment (a sum of spin and orbital contributions) for the $(\text{Fe}_{1-x}\text{Co}_x)_5\text{PB}_2$ system is presented in Fig. 4 together with the experimental results at low temperature (3 K).²⁸ Whereas the results presented here are based on the supercell approach²⁸, in our previous work one can find the corresponding $m(x)$ plots based on the virtual crystal approximation (VCA) and coherent potential approximation (CPA). The calculated and experimental $m(x)$ curves presented in Fig. 4 stay in good qualitative agreement, showing a linear decrease of magnetic moment with Co concentration. Nevertheless, they differ by about $0.5 - 1.0 \mu_B/\text{f.u.}$, where the lower values come from measurements. The reasons for this discrepancy should be sought on both experimental and theoretical sides. Looking at the experiment, it is worth noting that the samples produced in this work are slightly non-stoichiometric and with a small amount of impurities.²⁸ Our measurements at 3 K for a powder sample of Fe_5PB_2 showed a total magnetic moment equal to $8.29 \mu_B/\text{f.u.}$ in comparison to $8.6 \mu_B/\text{f.u.}$ obtained by Lamichane *et al.* for a Fe_5PB_2 single crystal at 2 K.²⁶ It leads us to the conclusion that the magnetic moments we have measured may be slightly underestimated. The calculated total magnetic moment of Fe_5PB_2 ($8.85 \mu_B/\text{f.u.}$) using GGA is closer to the result obtained for the single crystal than for the powder sample. The discrepancy between the result of GGA calculations and single crystal measurements can then be attributed to the insufficiency of the GGA in description of correlations, however the calculations still provide an acceptable level of agreement with experiment.

The calculated spin, orbital, and total magnetic moments (m_s , m_l , m) for Fe_5PB_2 and Co_5PB_2 are collected in Table II. For Fe_5PB_2 the calculated magnetic moments on Fe_1 and Fe_2 sites are equal to 1.81 (1.62) and 2.16 (2.16) μ_B , respectively, where in parentheses are given estimations from the magnetic hyperfine fields.⁵⁶ The induced spin magnetic moments on P and B are relatively small and oriented antiparallel to the dominant

$3d$ moments on Fe/Co. The total magnetic moments of Fe_5PB_2 and Co_5PB_2 are almost entirely of spin character, where the $3d$ orbital magnetic moments (m_l 's) are nearly quenched. The m_l 's of Fe_1 and Fe_2 of the Fe_5PB_2 (calculated for the [001] quantization axis) are equal to $0.033 \mu_B$ and $0.052 \mu_B$, respectively. These values surround the m_l value calculated for bcc Fe ($0.043 \mu_B$) and are reduced in comparison to the experimental value for the bcc Fe ($0.086 \mu_B$).⁵⁷ The underestimation of the orbital magnetic moment in transition metals is recognized as a general weakness of the LDA and GGA. Finally, almost no orbital contributions are observed for P and B atoms ($m_l \sim 10^{-3} \mu_B$). The calculated m of Co_5PB_2 is equal to $2.20 \mu_B/\text{f.u.}$ ($0.44 \mu_B/\text{Co atom}$). For comparison, the experimental magnetic moment of hcp Co is equal to $1.67 \mu_B/\text{atom}$.⁵⁸ The calculated m_l 's of Co_1 and Co_2 of the Co_5PB_2 are equal to $0.011 \mu_B$ and $0.013 \mu_B$, respectively, and are one order of magnitude smaller than the m_l measured for hcp Co ($0.13 \mu_B$).⁵⁹ Although the theoretical values of magnetic moments for Co_5PB_2 have been presented above, the magnetic ground state of this system has not been unambiguously resolved, which will be discussed in the next section.

C. Curie Temperature of $(\text{Fe}_{1-x}\text{Co}_x)_5\text{PB}_2$

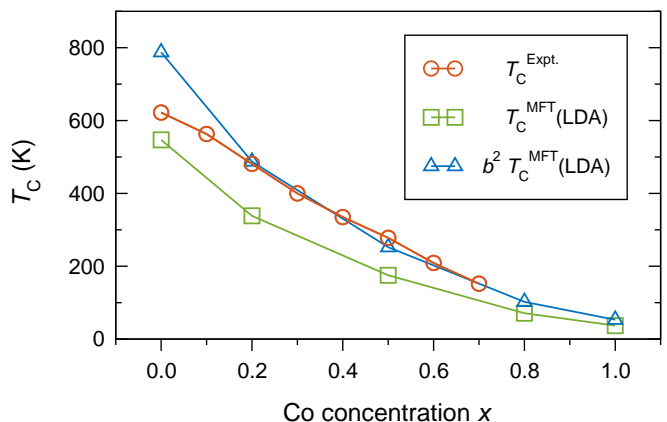


FIG. 5. The Curie temperatures as functions of Co concentration x in $(\text{Fe}_{1-x}\text{Co}_x)_5\text{PB}_2$. The theoretical $T_C^{\text{MFT(LDA)}}$ are calculated in the mean-field approximation with the FPLO5 code, using LDA functional, treating the chemical disorder with CPA, and modeling the paramagnetic state with DLM. The experimental T_C was defined from the inflection point of field cooled magnetization *versus* temperature measurements in a field of $\mu_0 H = 0.01 \text{ T}$.²⁸

The Curie temperatures ($T_C^{\text{MFT(LDA)}}$) calculated for the whole concentration range of the $(\text{Fe}_{1-x}\text{Co}_x)_5\text{PB}_2$ system within the mean-field theory and with the LDA functional are presented in Fig. 5. The observed overall decrease of the calculated $T_C^{\text{MFT(LDA)}}$ with increase of Co concentration is consistent with experimental observations.^{23,28} However, in the whole range in which it is pos-

sible to compare the MFT-LDA results with the experiment ($0.0 \leq x \leq 0.7$), theoretical values are smaller. For example, the calculated $T_C^{\text{MFT}}(\text{LDA})$ of Fe_5PB_2 is equal 547 K, whereas the corresponding experimental value is 622 K for the powder sample²⁸, or 655 ± 2 K for the single crystal.²⁶ This difference is due to the limitations of the MFT approach and insufficiency of the LDA in description of correlations. By calculating Heisenberg exchange interactions, one could extract accurate critical temperatures using the random phase approximation (RPA) or Monte Carlo simulations.^{60,61} The insufficiency of the LDA manifests in underestimated values of the calculated magnetic moments of Fe_5PB_2 ; $7.30 \mu_B/\text{f.u.}$ versus $8.6 \mu_B/\text{f.u.}$ from experiment for a single crystal.²⁶ As it has been shown in the previous subsection, a much better description of magnetic moments of Fe_5PB_2 in relation to the experimental result can be obtained by using the GGA functional instead LDA. Thus, we suggest that the negative effect on T_C^{MFT} coming from the limitations of the LDA can be partially corrected by using the correction parameter based on the magnetic moments obtained from GGA. In Heisenberg model, T_C^{MFT} is proportional to squared effective moment (m_{eff}^2). Defining $b = \frac{m_{\text{GGA}}}{m_{\text{LDA}}}$ the *corrected* Curie temperature is $b^2 T_C^{\text{MFT}}(\text{LDA})$, where in case of $(\text{Fe}_{1-x}\text{Co}_x)_5\text{PB}_2$ b is about 1.2. Figure 5 shows that for the region of intermediate Co concentrations the $b^2 T_C^{\text{MFT}}(\text{LDA})$ curve is in a better agreement with experiment than the uncorrected MFT-LDA results.

Unfortunately, we were unable to get experimental results of T_C for Co concentrations $x > 0.7$. Because of that, we can not unambiguously resolve the issue of the magnetic ground state of terminal composition Co_5PB_2 . Linear extrapolation of experimental magnetic moments for $(\text{Fe}_{1-x}\text{Co}_x)_5\text{PB}_2$ system suggests non-zero moment for Co_5PB_2 , see Fig. 4. On the contrary, linear extrapolation of the measured Curie temperature suggests a transition from ordered to disordered magnetic state at about $x = 0.9$, and therefore a non-magnetic ground state of Co_5PB_2 , see Fig. 5. Furthermore, experimental results reported by McGuire and Parker suggested absence of magnetic ordering for Co_5PB_2 .²³ From theoretical point of view, both uncorrected and corrected approaches show the non-zero values of T_C for Co-rich region ($T_C^{\text{MFT}}(\text{LDA}) = 37$ K for Co_5PB_2). Taking into account (1) the problems with synthesis of the Co_5PB_2 phase, (2) preliminary character of the measurements reported by McGuire and Parker, (3) issues mentioned in previous subsection regarding optimization of the structural model of Co_5PB_2 , and (4) limitations of LDA/GGA in description of correlations of Co-rich phases, we conclude that based on existing data the magnetic ground state of Co_5PB_2 can not be definitively determined.

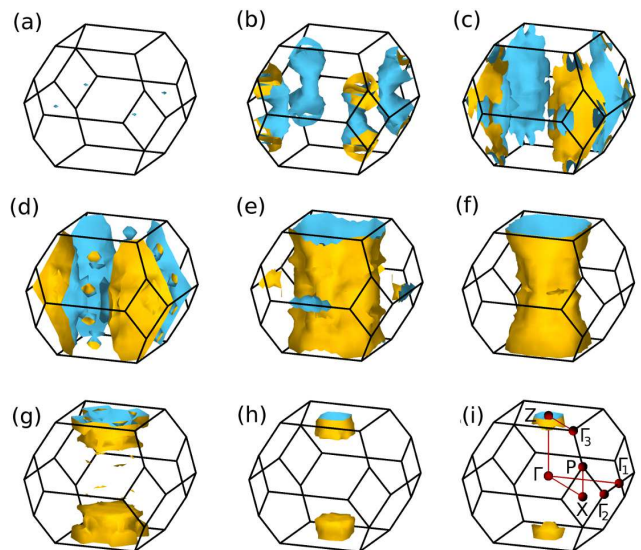


FIG. 6. (a)–(i) The nine sheets of the Fermi surface of Fe_5PB_2 . (i) The \mathbf{k} -path used to calculate the band structure plot. Inside the visible tubes the sheets (e) and (f) contain the invisible pockets centered at Γ . Calculations were done with the FPLO14 code using the PBE functional and treating the relativistic effects in a full 4-component formalism (including spin-orbit coupling).

D. Fermi Surface of Fe_5PB_2

Figure 6 presents the calculated Fermi surface (FS) of Fe_5PB_2 in a boundary of the first Brillouin zone. The FS of Fe_5PB_2 reflects the tetragonal symmetry of the crystal. The FS consists of nine sheets and is relatively complex. The states at the Fermi level (E_F) have a Fe $3d$ character, as can be read from the DOS plots in Fig. 3. The observed FS sheets can be divided into two groups. The first group consists of four nested sheets of hole-type, see panels (a)–(d) of Fig. 6, and the second group includes the remaining five sheets of electron-type nested in a multiwalled way around the high symmetry point Z , see panels (e)–(i) of Fig. 6. While the sheets (c)–(f) form rather tubular shapes, allowing for open orbits along the symmetry axis, the remaining sheets, (a)–(b) and (g)–(i), take the form of pockets enabling only for closed FS orbits.⁶² Because the band structure was calculated with spin-orbit coupling, the FS sheets cannot be unambiguously attributed to a particular spin channel.

E. Magnetocrystalline Anisotropy of Fe_5PB_2

The results of investigating the MAE of Fe_5PB_2 carried out in this work are: the band structure in vicinity of the Fermi level, one- and two-dimensional \mathbf{k} -resolved MAE plots, and the cross-section of FS. Our inquiry is complemented by considerations of MAE engineering, as for example reduction of total magnetic moment. The calcu-

lated MAE of the Fe_5PB_2 is 0.52 MJ m^{-3} . It indicates a uniaxial magnetocrystalline anisotropy with an easy axis along the tetragonal axis. This result stays in a good agreement with the experimental value of anisotropy constant measured at 2 K (0.50 MJ m^{-3}) and with the previous theoretical findings (0.46 MJ m^{-3}).²⁶ Previously reported results for Fe_5PB_2 show that K_1 first increases with temperature starting from 2 K up to about 100 K and then decreases to zero at T_C .²⁶ The well known origin of the magnetocrystalline anisotropy is the spin-orbit coupling, which is taken into account in the fully relativistic full potential calculations. In comparison with scalar relativistic approach, the fully relativistic one results in additional splitting of the electronic bands. Since the spin-orbit coupling constant of $3d$ -metals is of the order of 0.05 eV, the spin-orbit splitting also does not exceed this value. The spin-orbit splitting leads to slightly different band structures for different quantization axes (e.g. for the orthogonal [001] and [100] axes). Figure 7 presents the band structures calculated for Fe_5PB_2 in the proximity of E_F , together with the MAE contributions per \mathbf{k} -point obtained with the magnetic force theorem^{63–65} from the formula:

$$\begin{aligned} \text{MAE} &= E(\theta = 90^\circ) - E(\theta = 0^\circ) = \\ &= \sum_{\text{occ}'} \epsilon_i(\theta = 90^\circ) - \sum_{\text{occ}''} \epsilon_i(\theta = 0^\circ), \quad (6) \end{aligned}$$

where θ is an angle between the magnetization direction and the c axis, $E(\theta)$ is a total energy for a specific direction; and ϵ_i is the band energy of the i th state. The spin-orbit splitting is most easily observed for the energy window of a tenth eV around E_F . The \mathbf{k} -point resolved MAE takes positive and negative values, depending on the spin and orbital character of the bands near the Fermi energy. Generally, negative MAE-contributions coincide with occupied bands for a [100] spin quantization axis (solid red line) being pushed below corresponding bands for a [001] spin quantization axis (dashed blue line), and vice versa for positive contributions. For example, at the Z-point, there is a negative MAE contribution and at approximately -0.3 eV one can observe a solid red line below the dashed blue line. A more detailed analysis of the MAE contributions is in principle straight forward but somewhat complicated due to the complex band structure. Nevertheless, one can clearly observe the characteristic jumps where the bands cross E_F , confirming the usual behavior that the MAE is determined by the electronic structure around the Fermi energy. Thus, controlling the MAE around E_F also allows for control of the MAE, as is practically possible, for example, via alloying.

The same form of presentation of the \mathbf{k} -resolved MAE, as we have shown in Fig. 7, dominates in literature. However, it is possible to plot the MAE(\mathbf{k}) data within a three dimensional Brillouin zone, similar like the FS. Recently, the 3D MAE(\mathbf{k}) maps were presented for $(\text{Fe}_{1-x}\text{Co}_x)_2\text{B}$ and FeNi.^{17,66} In Fig. 8 (a) we show a cross-section of the MAE(\mathbf{k}) (single plane going trough the Γ -point). The

selected profile is perpendicular to the easy axis [001], crosses the high symmetry point Γ , and is limited by the Brillouin zone boundaries. The MAE(\mathbf{k}) cross-section is a relatively complicated map of symmetric regions consisting of positive and negative contributions. The MAE contributions observed in Fig. 8 along the orthogonal axes [100] and [010] are not equal, because the [100] direction is distinguished as quantization axis resulting in breaking of the four-fold symmetry. As the E_F is an upper integration boundary of total MAE, the FS sheets coincide with sharp changes in the \mathbf{k} -resolved MAE contributions. It can be seen in Fig. 8 (b), where the MAE(\mathbf{k}) 2D plot is overlapped by the corresponding section of the FS. As many of \mathbf{k} -resolved MAE contributions is in order of 10^{-3} eV per \mathbf{k} -point, the total MAE value of about 10^{-4} eV/f.u. ($83 \mu\text{eV/f.u.}$ or 0.52 MJ m^{-3}) indicates a fine compensation of many bigger components. Unfortunately, this extra fine compensation and the complexity of the MAE(\mathbf{k}) makes the ways to increase the MAE of the material difficult to predict.

F. Fully Relativistic Fixed Spin Moment Calculations for Fe_5PB_2

The MAE value for Fe_5PB_2 (0.52 MJ m^{-3}) is calculated with the equilibrium value of the magnetic moment ($8.85 \mu_B/\text{f.u.}$). In the fixed spin moment (FSM) method³⁴ the value of spin magnetic moment is considered as a parameter. The fully relativistic implementation of FSM method allows to calculate the MAE as a function of spin magnetic moment. Previously, we presented the MAE results as a function of FSM and Co concentration for the $(\text{Fe}_{1-x}\text{Co}_x)_2\text{B}$ alloys.¹⁹ Figure 9 presents the evolution of the MAE with the total magnetic moment m for the Fe_5PB_2 , together with the previous results for Fe_5SiB_2 .²⁴ The two MAE(m) plots are similar in shape. Going down from an equilibrium m the corresponding MAE first increases, then it reaches maximum, to decrease finally to zero at m equals zero. For Fe_5PB_2 the maximum MAE(m) is 1.94 MJ m^{-3} for a fixed total magnetic moment of $6.7 \mu_B/\text{f.u.}$, which means that the optimal magnetic moment has to be reduced by about 25% with respect to the equilibrium value ($8.85 \mu_B/\text{f.u.}$). Thus, the question arises, how to stabilize this reduction. A simple solution would be alloying the magnetic Fe by a non-magnetic element, which often results in a linear decrease of magnetization. However, alloying with a new element can severely affect the band structure, which would change also the expected value of the MAE. The smallest impact on the electronic structure should have substitutions chemically most similar to Fe and for this purpose we suggest Ru and Os of the Fe group. Another strategy could be alloying of Fe ($Z_{\text{Fe}} = 26$) with two elements at the same time, e.g. Cr ($Z_{\text{Cr}} = 24$) and Ni ($Z_{\text{Ni}} = 28$), keeping a constant number of the valence electrons, which should affect the band structure the least. The above considerations, however,

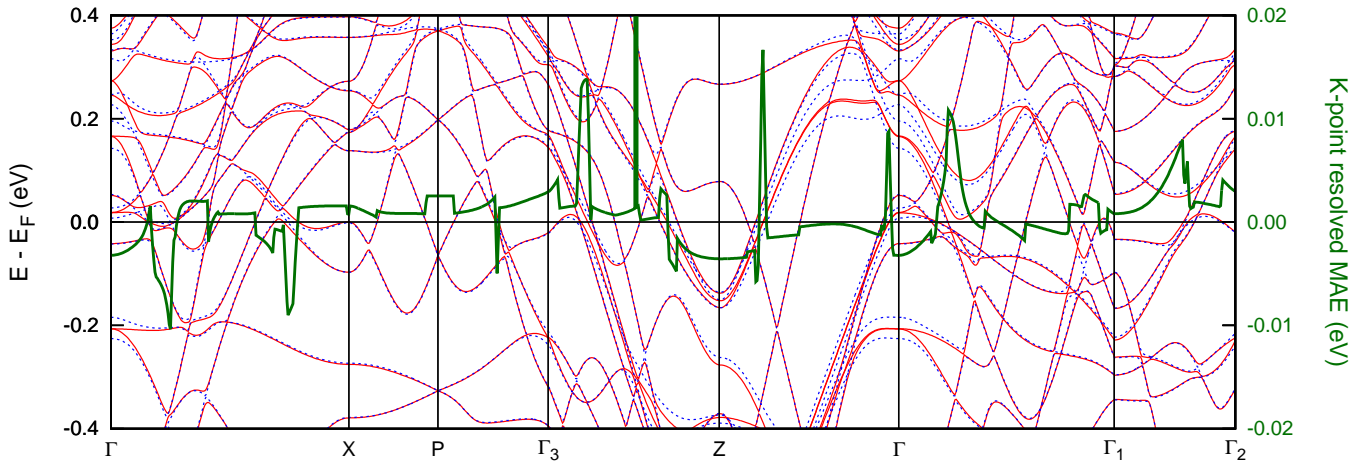


FIG. 7. The band structure of Fe_5PB_2 calculated for quantization axes [100] (solid red lines) and [001] (dashed blue lines), together with the MAE contribution of each \mathbf{k} -point (thick green line) as obtained by the magnetic force theorem. The high symmetry points are presented within Brillouin zone in Fig. 6 (i). Calculations were done with the FPLO14 code using the PBE functional and treating the relativistic effects in a full 4-component formalism (including spin-orbit coupling).

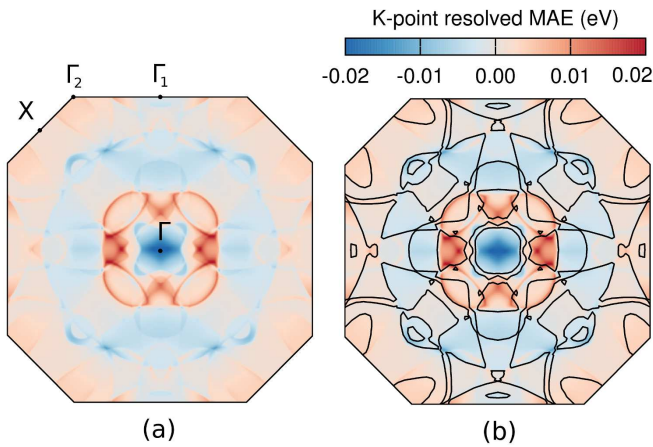


FIG. 8. (a) The cross-section of the \mathbf{k} -resolved MAE with (b) the overlapped cross-section of the Fermi surface (black lines) for the Fe_5PB_2 . The results of MAE(\mathbf{k}) are obtained by the magnetic force theorem within the FPLO14 code using the PBE functional and treating the relativistic effects in a full 4-component formalism (including spin-orbit coupling).

take into account only the band structure and neglect further issues like the crystal structure and size of the atoms, for example.

G. Magnetocrystalline Anisotropy of $(\text{Fe}_{1-x}\text{Co}_x)_5\text{PB}_2$

The effect of Fe/Co alloying on the MAE is not obvious in advance, whereby the first-principles calculations are of great value in predicting the results, as has been shown previously for the $(\text{Fe}_{1-x}\text{Co}_x)_2\text{B}$ ¹⁷ and $(\text{Fe}_{1-x}\text{Co}_x)_5\text{SiB}_2$ ²⁴ alloys. Figure 10 presents the MAE(x) dependence for the $(\text{Fe}_{1-x}\text{Co}_x)_5\text{PB}_2$ system as

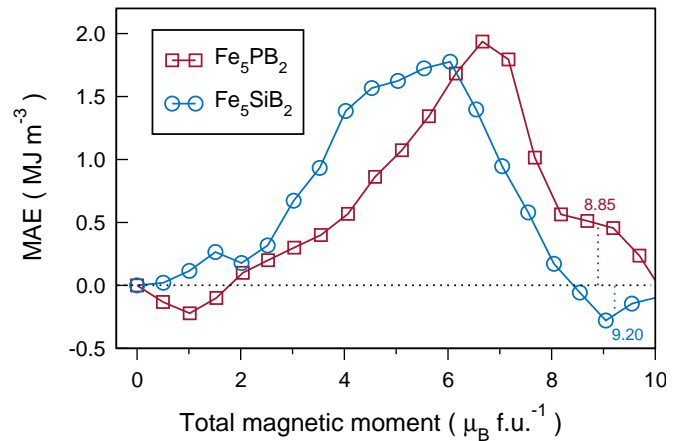


FIG. 9. MAE as function of total magnetic moment (m_S+m_L) for Fe_5PB_2 and Fe_5SiB_2 ²⁴ as calculated with fixed spin moment (FSM) method with the FPLO14 code using the PBE functional and treating the relativistic effects in a full 4-component formalism (including spin-orbit coupling). The equilibrium values of magnetic moments are denoted with dotted lines.

calculated with use of the supercell method. The MAE calculations based on the supercell method proved to be one of the most accurate method for evaluation the MAE.¹⁸ However, our calculations were limited by computational challenges of the supercell method. Thus, in practice we were able to consider only a relatively small number of configurations, see Sec. II A. The scattering of individual data points for $x = 0.2$ and $x = 0.8$ is in a similar range as observed by Däne *et al.*¹⁸ or Steiner *et al.*³⁶ and shows that an averaging for several configurations is needed for accurate results. In Fig. 10 the regions of positive and negative MAE (of perpendicular and in-plane anisotropy) are separated at Co concentra-

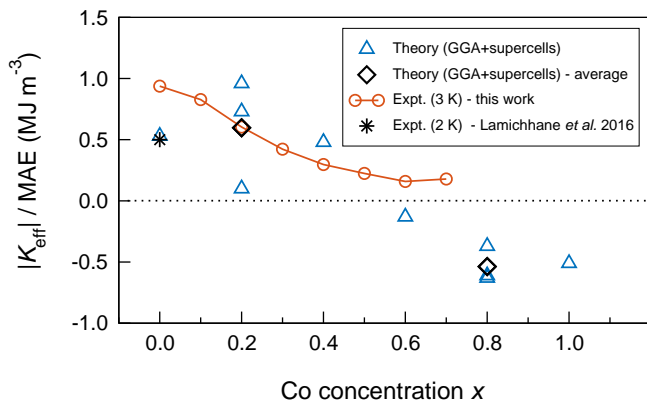


FIG. 10. The experimental effective anisotropy constant $|K_{\text{eff}}|$ of the $(\text{Fe}_{1-x}\text{Co}_x)_5\text{PB}_2$ system at 3 K (the sign of K_{eff} is not considered), together with the magnetocrystalline anisotropy energy MAE values as calculated with the FPLO14 code. In calculations the supercell method for modeling of chemical disorder and the PBE functional were used. The relativistic effects were treated in a full 4-component formalism (including spin-orbit coupling). (for x equal to 0.2 and 0.8 several inequivalent supercells are considered). For comparison the value of K_1 measured by Lamichhane *et al.* for Fe_5PB_2 .²⁶

tion $x \simeq 0.5$. The calculated MAE is equal 0.52 MJ m^{-3} for Fe_5PB_2 and -0.51 MJ m^{-3} for Co_5PB_2 . Whereas, the anisotropy value close to zero, observed for $x \simeq 0.5$, indicates a good soft magnetic material. Figure 10 presents also the low temperature measurements of the effective anisotropy constant $|K_{\text{eff}}|$ carried out at 3 K for several $(\text{Fe}_{1-x}\text{Co}_x)_5\text{PB}_2$ compositions within the boundaries of $0.0 \leq x \leq 0.7$. The value of $|K_{\text{eff}}|$ is the highest (0.94 MJ m^{-3}) for Fe_5PB_2 and the lowest for a Co concentration $x \sim 0.6$. $|K_{\text{eff}}|$ measured for Fe_5PB_2 is significantly larger than the $K_1 = 0.5 \text{ MJ m}^{-3}$ measured at 2 K for the single crystal.²⁶ The decrease of $|K_{\text{eff}}|$ with x is in agreement with the previous measurements for $(\text{Fe}_{0.8}\text{Co}_{0.2})_5\text{PB}_2$ suggesting that 20% Co substitution reduces the anisotropy field.²³ Previously we also showed the corresponding $|K_{\text{eff}}|$ results for the $\text{Fe}_5\text{Si}_{1-x}\text{P}_x\text{B}_2$ system.²⁷ The presented values of $|K_{\text{eff}}|$ for Fe_5PB_2 were $\sim 0.9 \text{ MJ m}^{-3}$ at 10 K and $\sim 0.65 \text{ MJ m}^{-3}$ at 300 K.²⁷ Notice that LAS is unable to determine the sign of $|K_{\text{eff}}|$ and thus the negative values of MAE predicted for $x \gtrsim 0.6$ cannot be confirmed by this method. Other methods, such as magnetometry measurements in different directions for single crystals or torque magnetometry would be preferable. Here, single crystals were not available, and up to 10 wt% of impurities were present in the samples. Therefore, given the limitation in the model and the starting material the results presented from these should be seen as semi-quantitative. Taking into account the limitations of the LAS and the supercell method, the differences between theoretical and measured MAE(x) results are acceptable. We conclude, that Co alloying of Fe_5PB_2 is not a good strategy to increase the MAE of

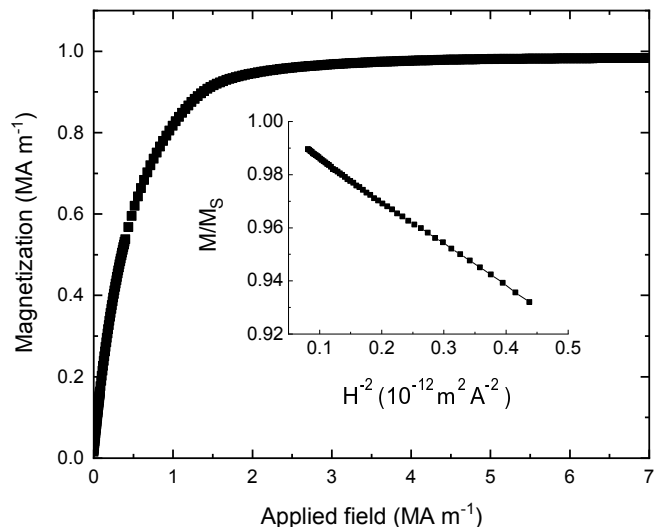


FIG. 11. Magnetization (M) as a function of applied field (H) measured for Fe_5PB_2 at 3 K. The inset shows a normalized magnetization (M/M_S) as a function of $1/H^2$.

this system.

A typical magnetization (M) versus applied field (H) curve measured at 3 K is shown in Fig. 11. The inset of Fig. 11 presents a plot of M/M_S versus $1/H^2$ as used to determine the $|K_{\text{eff}}|$ within the LAS method. More details on the implementation of the LAS method can be found in Sec. II B.

H. Doping Fe_5PB_2 with 5d Elements

One of the methods of tailoring the MAE is doping with 5d elements.^{19,67} Previously, we have confirmed that the 5d elements can significantly affect the MAE due to a large spin-orbit coupling.¹⁹ From the $\text{Fe}_5\text{Si}_{1-x}\text{P}_x\text{B}_2$ and $(\text{Fe}_{1-x}\text{Co}_x)_5\text{PB}_2$ systems, the highest MAE is found in the Fe_5PB_2 phase.²⁷ Thus, it is considered as the parental compound for a further MAE engineering. The MAE of $(\text{Fe}_{0.95}\text{X}_{0.05})_5\text{PB}_2$ compounds ($X = 5d$ elements) is calculated using the supercell method. The results are shown in Fig. 12, with the 5d element marked on the x axis and dashed line indicating the MAE of undoped Fe_5PB_2 . The 5d doping has sometimes beneficial and sometimes adverse effect on MAE.^{35,68,69} Significant increase of MAE is observed for W or Re doping, similar like in the case of $(\text{Fe}_{1-x}\text{Co}_x)_2\text{B}$ alloys investigated experimentally in our previous work¹⁹. The MAE grows from 0.52 MJ m^{-3} for Fe_5PB_2 to about 1.1 MJ m^{-3} for the compositions with W or Re, with 5% Fe substitution. Previously we have shown, that the increase in MAE observed for W and Re dopants is mainly due to the strong spin-orbit coupling of the 5d atoms, however other variations in electronic structure also affect the MAE.¹⁹ Although in our calculations the 5d elements are initially considered as non-magnetic, the dopants undergo spin

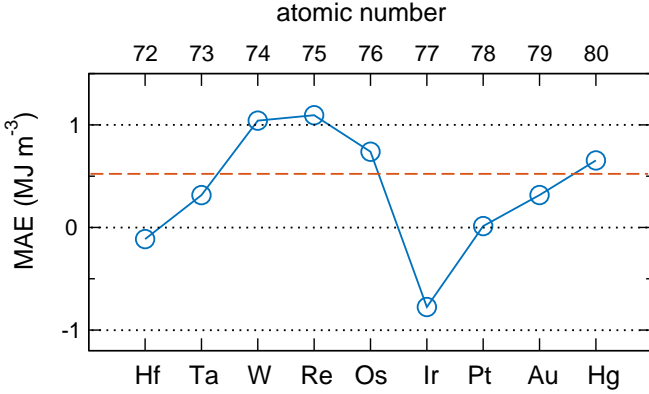


FIG. 12. MAE for various $5d$ elements X in $(\text{Fe}_{0.95}\text{X}_{0.05})_5\text{PB}_2$ as calculated with supercell method. Calculations were done with the FPLO14 code using the PBE functional and treating the relativistic effects in a full 4-component formalism (including spin-orbit coupling). The dashed line indicates the MAE of Fe_5PB_2 (0.52 MJ m^{-3}) for comparison.

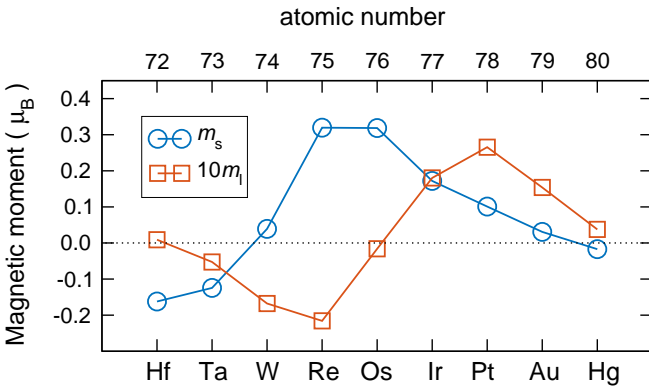


FIG. 13. Spin (m_s) and orbital (m_l) magnetic moments of $5d$ transition metal impurities X in $(\text{Fe}_{0.95}\text{X}_{0.05})_5\text{PB}_2$ as calculated for spin quantization axis along the c -axis. Supercell calculations were done with the FPLO14 code using the PBE functional and treating the relativistic effects in a full 4-component formalism (including spin-orbit coupling).

polarization in a ferromagnetic medium and contribute to the total magnetic moment of the system. The calculated spin and orbital magnetic moments on $5d$ impurity show clear trend along the increasing atomic number of $5d$ element, see Fig. 13. The spin magnetic moment of $5d$ impurities are antiparallel to the Fe moments in the early $5d$ series, while they are parallel in the late $5d$ series. Corresponding trends for $5d$ atoms in magnetic $3d$ hosts have been found previously computationally^{70,71} and experimentally.⁷²

IV. SUMMARY AND CONCLUSIONS

Our considerations began with a detailed theoretical analysis of the Fe_5PB_2 compound. The Fe $3d$ orbitals

are dominant in the valence band and responsible for the formation of large magnetic moments. For the Fe_5PB_2 the fully relativistic band structure in the vicinity of Fermi level was considered to better understand the origin of the high value of magnetocrystalline anisotropy energy (MAE). The calculated Fermi surface requires experimental confirmation. The results of fully relativistic fixed spin moment calculations suggested that reduction of the magnetic moment of Fe_5PB_2 should induce about fourfold increase of the MAE. For practical realization of magnetic moment reduction it is suggested to alloy Fe with a non-magnetic element Ru or Os from the Fe group, or to partially replace Fe with two elements at once, Cr and Ni, for example, keeping constant number of valence electrons.

Three critical parameters for technological applications: saturation magnetization (M_S), Curie temperature (T_C), and MAE were calculated for the whole concentration range between Fe_5PB_2 and Co_5PB_2 . The calculated M_S and T_C decreased with Co concentration and for the terminal composition Co_5PB_2 a weakly ordered magnetic ground state was predicted. The calculated $M(x)$ and $T_C(x)$ were in decent agreement with the measurements, although the ferromagnetic ground state of Co_5PB_2 is questionable. The Co doping in $(\text{Fe}_{1-x}\text{Co}_x)_5\text{PB}_2$ system gives the possibility of tuning the T_C in a range from about six hundred kelvins to almost down to zero. The calculated MAE was positive for Fe_5PB_2 , negative for Co_5PB_2 , and went through zero around 50% Co concentration. This picture of $\text{MAE}(x)$ behavior was in overall agreement with the experimental study of the effective anisotropy constant $|K_{\text{eff}}|$ for the $(\text{Fe}_{1-x}\text{Co}_x)_5\text{PB}_2$ alloys. The measurements showed the highest $|K_{\text{eff}}|$ value for stoichiometric Fe_5PB_2 which decreased with Co doping. We concluded then that Co alloying is not a good strategy to increase the MAE of Fe_5PB_2 alloy. The measured $|K_{\text{eff}}|$ of about 0.94 MJ m^{-3} at 3 K was, however, the highest value obtained so far for Fe_5PB_2 , giving a hope for potential application of its other alloys. It was also calculated how the 5% doping of Fe with $5d$ elements affects the MAE of the Fe_5PB_2 . It was shown that Fe_5PB_2 doping with W or Re results in significant increase of the magnetocrystalline anisotropy energy.

ACKNOWLEDGMENTS

MW and JR acknowledge the financial support from the Foundation of Polish Science grant HOMING. The HOMING programme is co-financed by the European Union under the European Regional Development Fund. JC and MS acknowledge the financial support from the Swedish Research Council. DH, PS, KG acknowledge Swedish Foundation for Strategic Research for financial support. Part of the computations were performed on resources provided by the Poznań Supercomputing and Networking Center (PSNC). We thank Bar-

tosz Wasilewski for help with language editing and Dr

Jakub Kaczkowski for reading the manuscript and helpful discussion.

-
- * Corresponding author: werwinski@ifmpan.poznan.pl
- ¹ K. Bourzac, *Technology Review* **114**, 58 (2011).
 - ² D. Niarchos, G. Giannopoulos, M. Gjoka, C. Sarafidis, V. Psycharis, J. Ruzs, A. Edström, O. Eriksson, P. Toson, J. Fidler, E. Anagnostopoulou, U. Sanyal, F. Ott, L.-M. Lacroix, G. Viau, C. Bran, M. Vazquez, L. Reichel, L. Schultz, and S. Fähler, *JOM* **67**, 1318 (2015).
 - ³ S. Hirosawa, *Journal of the Magnetism Society of Japan advpub*, 85 (2015).
 - ⁴ R. Skomski and J. Coey, *Scripta Materialia* **112**, 3 (2016).
 - ⁵ D. Li, D. Pan, S. Li, and Z. Zhang, *Science China Physics, Mechanics & Astronomy* **59**, 617501 (2016).
 - ⁶ S. Hirosawa, M. Nishino, and S. Miyashita, *Advances in Natural Sciences: Nanoscience and Nanotechnology* **8**, 013002 (2017).
 - ⁷ O. Gutfleisch, M. A. Willard, E. Brück, C. H. Chen, S. G. Sankar, and J. P. Liu, *Advanced Materials* **23**, 821 (2011).
 - ⁸ S. Fähler, U. K. Röbber, O. Kastner, J. Eckert, G. Eggeler, H. Emmerich, P. Entel, S. Müller, E. Quandt, and K. Albe, *Advanced Engineering Materials* **14**, 10.
 - ⁹ T. Burkert, L. Nordström, O. Eriksson, and O. Heinonen, *Phys. Rev. Lett.* **93**, 027203 (2004).
 - ¹⁰ G. Andersson, T. Burkert, P. Warnicke, M. Björck, B. Sanyal, C. Chacon, C. Zlotea, L. Nordström, P. Nordblad, and O. Eriksson, *Phys. Rev. Lett.* **96**, 037205 (2006).
 - ¹¹ Y. Kota and A. Sakuma, *Applied Physics Express* **5**, 113002 (2012).
 - ¹² I. Turek, J. Kudrnovský, and K. Carva, *Phys. Rev. B* **86**, 174430 (2012).
 - ¹³ E. K. Delczeg-Czirjak, A. Edström, M. Werwiński, J. Ruzs, N. V. Skorodumova, L. Vitos, and O. Eriksson, *Phys. Rev. B* **89**, 144403 (2014).
 - ¹⁴ L. Reichel, G. Giannopoulos, S. Kauffmann-Weiss, M. Hoffmann, D. Pohl, A. Edström, S. Oswald, D. Niarchos, J. Ruzs, L. Schultz, and S. Fähler, *J. Appl. Phys.* **116**, 213901 (2014).
 - ¹⁵ L. Reichel, L. Schultz, D. Pohl, S. Oswald, S. Fähler, M. Werwiński, A. Edström, E. K. Delczeg-Czirjak, and J. Ruzs, *J. Phys.: Condens. Matter* **27**, 476002 (2015).
 - ¹⁶ M. D. Kuz'min, K. P. Skokov, H. Jian, I. Radulov, and O. Gutfleisch, *J. Phys.: Condens. Matter* **26**, 064205 (2014).
 - ¹⁷ K. D. Belashchenko, L. Ke, M. Däne, L. X. Benedict, T. N. Lamichhane, V. Taufour, A. Jesche, S. L. Bud'ko, P. C. Canfield, and V. P. Antropov, *Applied Physics Letters* **106**, 062408 (2015).
 - ¹⁸ M. Däne, S. K. Kim, M. P. Surh, D. Åberg, and L. X. Benedict, *J. Phys.: Condens. Matter* **27**, 266002 (2015).
 - ¹⁹ A. Edström, M. Werwiński, D. Iuşan, J. Ruzs, O. Eriksson, K. P. Skokov, I. A. Radulov, S. Ener, M. D. Kuz'min, J. Hong, M. Fries, D. Y. Karpenkov, O. Gutfleisch, P. Toson, and J. Fidler, *Phys. Rev. B* **92**, 174413 (2015).
 - ²⁰ W. Wallisch, J. Fidler, P. Toson, H. Sassik, R. Svagera, and J. Bernardi, *J. Alloys Compd.* **644**, 199 (2015).
 - ²¹ A. Iga, *Japanese Journal of Applied Physics* **9**, 415 (1970).
 - ²² I. A. Zhuravlev, V. P. Antropov, and K. D. Belashchenko, *Phys. Rev. Lett.* **115**, 217201 (2015).
 - ²³ M. A. McGuire and D. S. Parker, *J. Appl. Phys.* **118**, 163903 (2015).
 - ²⁴ M. Werwiński, S. Kontos, K. Gunnarsson, P. Svedlindh, J. Cedervall, V. Höglin, M. Sahlberg, A. Edström, O. Eriksson, and J. Ruzs, *Phys. Rev. B* **93**, 174412 (2016).
 - ²⁵ J. Cedervall, S. Kontos, T. C. Hansen, O. Balmes, F. J. Martinez-Casado, Z. Matej, P. Beran, P. Svedlindh, K. Gunnarsson, and M. Sahlberg, *J. Solid State Chem.* **235**, 113 (2016).
 - ²⁶ T. N. Lamichhane, V. Taufour, S. Thimmaiah, D. S. Parker, S. L. Bud'ko, and P. C. Canfield, *J. Magn. Magn. Mater.* **401**, 525 (2016).
 - ²⁷ D. Hedlund, J. Cedervall, A. Edström, M. Werwiński, S. Kontos, O. Eriksson, J. Ruzs, P. Svedlindh, M. Sahlberg, and K. Gunnarsson, *Phys. Rev. B* **96**, 094433 (2017).
 - ²⁸ J. Cedervall, E. Nonnet, D. Hedlund, L. Häggström, T. Ericsson, M. Werwiński, A. Edström, J. Ruzs, P. Svedlindh, K. Gunnarsson, and M. Sahlberg, *Inorg. Chem.* **57**, 777 (2018).
 - ²⁹ S. Rundqvist, *Acta Chemica Scandinavica* **16**, 1 (1962).
 - ³⁰ B. Lejeune, R. Barua, I. McDonald, A. Gabay, L. Lewis, and G. Hadjipanayis, *J. Alloys Compd.* **731**, 995 (2018).
 - ³¹ K. Koepernik and H. Eschrig, *Phys. Rev. B* **59**, 1743 (1999).
 - ³² J. P. Perdew, K. Burke, and M. Ernzerhof, *Phys. Rev. Lett.* **77**, 3865 (1996).
 - ³³ P. E. Blöchl, O. Jepsen, and O. K. Andersen, *Phys. Rev. B* **49**, 16223 (1994).
 - ³⁴ K. Schwarz and P. Mohn, *J. Phys. F: Met. Phys.* **14**, L129 (1984).
 - ³⁵ A. Edström, *Phys. Rev. B* **96**, 064422 (2017).
 - ³⁶ S. Steiner, S. Khmelevskiy, M. Marsmann, and G. Kresse, *Phys. Rev. B* **93**, 224425 (2016).
 - ³⁷ K. Koepernik, B. Velický, R. Hayn, and H. Eschrig, *Phys. Rev. B* **55**, 5717 (1997).
 - ³⁸ B. L. Gyorffy, A. J. Pindor, J. Staunton, G. M. Stocks, and H. Winter, *J. Phys. F: Met. Phys.* **15**, 1337 (1985).
 - ³⁹ K. Sato, P. H. Dederics, and H. Katayama-Yoshida, *Europhysics Letters (EPL)* **61**, 403 (2003).
 - ⁴⁰ J. Kudrnovský, I. Turek, V. Drchal, F. Máca, P. Weinberger, and P. Bruno, *Phys. Rev. B* **69**, 115208 (2004).
 - ⁴¹ V. Heine, J. H. Samson, and C. M. M. Nex, *Journal of Physics F: Metal Physics* **11**, 2645 (1981).
 - ⁴² P. Soven, *Phys. Rev.* **156**, 809 (1967).
 - ⁴³ J. P. Perdew and Y. Wang, *Phys. Rev. B* **45**, 13244 (1992).
 - ⁴⁴ K. Momma and F. Izumi, *J. Appl. Crystallogr.* **41**, 653 (2008).
 - ⁴⁵ B. Carlsson, M. Gölin, and S. Rundqvist, *J. Solid State Chem.* **8**, 57 (1973).
 - ⁴⁶ J. Rodríguez-Carvajal, *Physica B: Condensed Matter* **192**, 55 (1993).
 - ⁴⁷ H. Rietveld, *J. Appl. Crystallogr.* **2**, 65 (1969).

- ⁴⁸ T. J. B. Holland and S. A. T. Redfern, *Mineralogical Magazine* **61**, 65 (1997).
- ⁴⁹ S. Chikazumi, C. D. Graham, and S. Chikazumi, *Physics of ferromagnetism*, 2nd ed., The international series of monographs on physics No. 94 (Clarendon Press ; Oxford University Press, Oxford : New York, 1997).
- ⁵⁰ S. V. Andreev, M. I. Bartashevich, V. I. Pushkarsky, V. N. Maltsev, L. A. Pamyatnykh, E. N. Tarasov, N. V. Kudrevatykh, and T. Goto, *J. Alloys Compd.* **260**, 196 (1997).
- ⁵¹ H. Zhang, D. Zeng, and Z. Liu, *J. Magn. Magn. Mater.* **322**, 2375 (2010).
- ⁵² W. F. Brown, *Phys. Rev.* **58**, 736 (1940).
- ⁵³ P. Haas, F. Tran, and P. Blaha, *Phys. Rev. B* **79**, 085104 (2009).
- ⁵⁴ M. Ropo, K. Kokko, and L. Vitos, *Phys. Rev. B* **77**, 195445 (2008).
- ⁵⁵ M. Zelený, D. Legut, and M. Šob, *Phys. Rev. B* **78**, 224105 (2008).
- ⁵⁶ L. Häggström, R. Wäppling, T. Ericsson, Y. Andersson, and S. Rundqvist, *J. Solid State Chem.* **13**, 84 (1975).
- ⁵⁷ C. T. Chen, Y. U. Idzerda, H.-J. Lin, N. V. Smith, G. Meigs, E. Chaban, G. H. Ho, E. Pellegrin, and F. Sette, *Phys. Rev. Lett.* **75**, 152 (1995).
- ⁵⁸ R. A. Reck and D. L. Fry, *Phys. Rev.* **184**, 492 (1969).
- ⁵⁹ R. M. Moon, *Phys. Rev.* **136**, A195 (1964).
- ⁶⁰ E. Şaşıoğlu, L. M. Sandratskii, and P. Bruno, *J. Appl. Phys.* **98**, 063523 (2005).
- ⁶¹ J. Ruzs, I. Turek, and M. Diviš, *Phys. Rev. B* **71**, 174408 (2005).
- ⁶² J. M. Ziman, *Contemporary Physics* **4**, 81 (1962).
- ⁶³ A. I. Liechtenstein, M. I. Katsnelson, V. P. Antropov, and V. A. Gubanov, *J. Magn. Magn. Mater.* **67**, 65 (1987).
- ⁶⁴ X. Wang, D.-s. Wang, R. Wu, and A. J. Freeman, *J. Magn. Magn. Mater.* **159**, 337 (1996).
- ⁶⁵ R. Wu and A. J. Freeman, *J. Magn. Magn. Mater.* **200**, 498 (1999).
- ⁶⁶ M. Werwiński and W. Marciniak, *J. Phys. D: Appl. Phys.* **50**, 495008 (2017).
- ⁶⁷ I. Khan and J. Hong, *Current Applied Physics* **18**, 526 (2018).
- ⁶⁸ S. Ayaz Khan, P. Blaha, H. Ebert, J. Minár, and O. Šipr, *Phys. Rev. B* **94**, 144436 (2016).
- ⁶⁹ A. Edström, *Theoretical and Computational Studies on the Physics of Applied Magnetism : Magnetocrystalline Anisotropy of Transition Metal Magnets and Magnetic Effects in Elastic Electron Scattering*, Ph.D. thesis (2016).
- ⁷⁰ H. Akai, *Hyperfine Interact* **43**, 253 (1988).
- ⁷¹ P. H. Dederichs, R. Zeller, H. Akai, and H. Ebert, *J. Magn. Magn. Mater.* **100**, 241 (1991).
- ⁷² R. Wienke, G. Schütz, and H. Ebert, *J. Appl. Phys.* **69**, 6147 (1991).